

Analysis of Full-scale Load Tests on Bored Piles Socketed in Weathered Rock: A Case Study of the Subsoils of Phnom Penh Area

Khiahok Ing^{1,*} and Pongpipat Anantanasakul²

^{1,2} Department of Civil and Environmental Engineering, Faculty of Engineering, Mahidol University, Nakhon Pathom, THAILAND

*Corresponding author; E-mail address: khiahok.ing@student.mahidol.edu

Abstract

Construction of high-rise buildings in the city of Phnom Penh has increased significantly in the past decade. The typical subsurface conditions of this urban area consist of a complex sequence of fluvial deposits of sandy and clayey soils underlain by sedimentary rock. Bored piles socketed in the rock layer have primarily been used as the foundation systems for such high-rise buildings. However, the current design knowledge of large-capacity bored piles in these particular ground conditions is rather limited. Due to the availability of the experimental results of full-scale static load test and high-strain dynamic tests on large-diameter bored piles, the present study was undertaken to gain better insight into the load transfer mechanisms as well as the settlement response of such deep foundations. A 2D axisymmetric finite element analysis was also performed to simulate the load-settlement relations obtained from the static load test. The experimental results indicated that skin friction significantly contributes to the pile mobilized capacities, to a degree much more than what previously thought by the local geotechnical community. The numerical predictions of the finite element model were observed to match the experimental load-settlement relationships fairly precisely. Parameter values of the soils and rocks that result in such realistic simulations of the pile response are presented herein.

Keywords: Bored pile, Load-transfer mechanism, Pile socketed in rock, Pile load test, Settlement analysis, Axisymmetric finite element model

1. Introduction

Construction of high-rise buildings in the city of Phnom Penh has increased significantly over the past decade. The typical

subsurface conditions of this urban area consist of a complex sequence of fluvial deposits of sandy and clayey soils underlain by sedimentary rock. Bored piles socketed in the rock layer have primarily been used as the foundation systems for such high-rise buildings. For the current local design practice, a bored pile is usually considered “end-bearing pile” with the shaft resistances of both soil and rock portions completely ignored when it is installed into strong rock. For a pile installed in weak and weathered rock, the soil shaft resistance is still omitted and the ultimate capacity of the bored pile is the summation of the shaft resistance and the end-bearing of the rock-socketed portion. In general, limit-analysis methods are employed to determine the unit skin friction and end bearing of a bored pile in rock socket [1–2].

However, the results of static load tests on instrumented bored piles socketed in rock elsewhere exhibit rather complex load transfer mechanisms [3–5]. Chen et al. (2019) [6] studied the behavior of fully-instrumented bored piles constructed through soil and socketed into siltstone and reported significant contributions of the soil shaft resistance to the mobilized capacities. Aye et al. (2017) [7] also reported highly varying back-calculated values of unit skin friction and end bearing of piles socketed in sandstone and siltstone. Such variation is attributed to construction technique, rock quality and the degree to which the pile is mobilized. Some studies suggest that design of a bored pile socketed in rock should be governed by displacement rather than load carrying capacity. This is because the capacity is, in general, far in excess of the strength of the superstructure and the pile itself [8].



Fig. 1 Test site located in the central part of the Phnom Penh area

Due to the availability of the experimental results of full-scale load tests on large-diameter bored piles socketed in rock in the Phnom Penh area, the present study was undertaken to gain better insight into the load transfer mechanisms as well as the settlement response of such deep foundations. Axial forces in the instrumented test pile were analyzed, thus allowing for determination of the skin friction and end bearing components of the mobilized capacities. An axisymmetric finite element analysis of the axially loaded bored pile was also performed. The elastoplastic Hardening Soil (HS) model was used to predict the stress-strain and strength behavior of the upper sandy and clayey soil layers, while the sedimentary rock was represented by Hoek-Brown (HB) model. Parameter values of the soils and rocks that result in fairly realistic simulations of the pile response are presented, and recommendations toward design practice for large-diameter bored piles in the subsoil of the Phnom Penh area are made herewith.

2. Geological conditions of Phnom Penh area

The city of Phnom Penh is located in the southern part of Cambodia and it is situated at the confluence of the Mekong River, Bassac River and Tonle Sap River. As a result, seasonal flooding of these rivers significantly affects the subsoil conditions

of the Phnom Penh area. Such fluvial environments and activities have created a complex sequence of sandy and clayey soil deposits overlying weathered sedimentary rock. Touch et al. (2014) [9] categorized the subsoils of the Phnom Penh area into three parts, namely, the western, central and eastern parts. The subsoils of the western part mainly comprise of stiff to very stiff clay approximately 6-7 m thick overlying medium to very dense sand. The upper soil layers of the central part are a sequence of made ground, very soft to very stiff clay and hard silt with total thicknesses of about 27 m. Medium dense to very dense sand and stiff to very stiff clay layers can be found below the aforementioned soil layers. The eastern part consists of soft clay and silt layers 12 m thick. These soil layers are underlain by medium dense to very dense sand down to depths of 25-30 m [9].

3. Geotechnical investigation of test site

The present experimental program was part of the construction project of a high-rise residential building in the central part of the Phnom Penh area. One exploratory borehole, denoted as BH-02 and 65 m deep, was made to characterize the geotechnical conditions of the test site. Standard penetration tests (ASTM D1586) were performed using a self-tripping hammer.

When possible, undisturbed samples were collected using thin-walled tubes through rotary drilling with bentonite flushing. These retrieved undisturbed samples later underwent laboratory index, consolidation and strength tests. The index tests comprised of classification, particle-size distribution, moisture content, unit weight, specific gravity and consistency limits. Consolidation and strength tests included one-dimensional consolidation or oedometer tests, unconfined compression (UC) tests and consolidated-undrained (CU) triaxial compression tests. The results of such geotechnical investigation are in excellent agreement with the general geological conditions of the area. Six cohesive and cohesionless soil layers underlain by two sedimentary rock layers, as shown in Fig. 3, can be distinguished at the test site. The ground water level, measured in accordance with ASTM D4750 Standard, in the borehole was approximately 2.10 m below the ground surface.

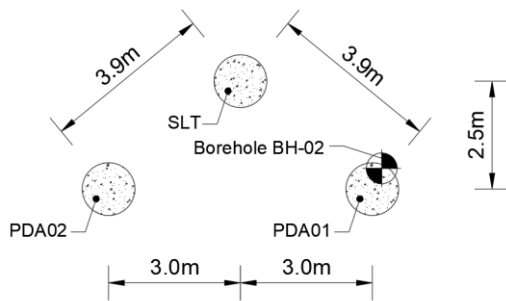


Fig. 2 Locations of static pile load test and high-strain dynamic or PDA tests at test site

4. Field load tests

4.1 Static pile load test

The test bored pile was located 3.90 m from Borehole BH-02 as shown in Fig. 2. It was 56.90 m deep and measured 1.2 m in diameter. The average concrete compressive strength at 28 days as determined from cylindrical specimens was approximately 32 MPa. The static load test denoted as SLT in the figure was performed in October 2020 with a maximum downward load at the head twice as large the design working load, i.e., $P_a = 12,800$ kN. The present full-scale test was carried out in two load cycles. Axial loads (P) for the first cycle were applied in eight increments, each within 30 minutes, until $P = P_a$ was attained. For the second cycle, the loading rate was doubled to achieve the maximum load of $P = 2P_a$ within the same period of time, i.e., four hours. For both test cycles, the respective maximum loads were kept constant for 24 hours and

they were later incrementally unloaded at the same rates as discussed before. The head settlement of test pile was monitored using four precision dial indicators during the course of load testing.

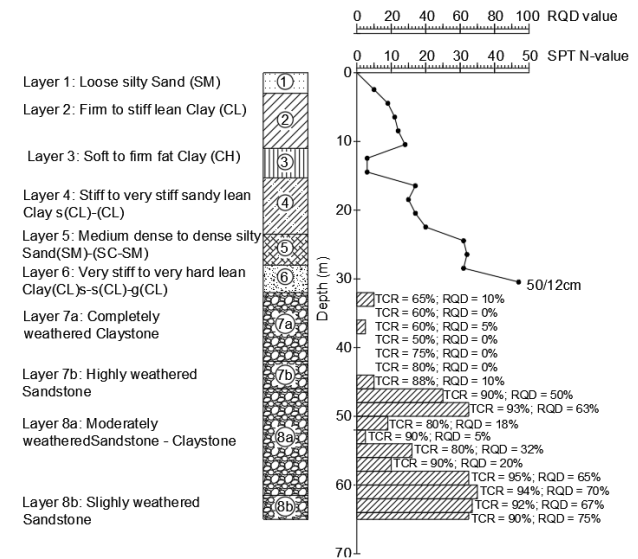


Fig. 3 Representative soil profile at test site as determined from borehole BH-02

The test pile was instrumented with 24 vibrating strain gauges (Geokon Model 4200) and three extensometers (GEOKON Model 1300 A-9). The strain gauges were attached to the reinforcing steel cage at various depths as shown in Fig. 4. It should be noted that three strain gauges were employed at each test depth or elevation so as to provide redundancy and to cross-check the experimental strain readings. The extensometers were installed in a tube embedded in the bored pile to investigate its shortening response under compressive loads both in the soil and rock layers. Prior to installation of the extensometers, the tube was employed to perform sonic logging tests to check the integrity of the test pile. This extensometer assemblage comprised of pneumatically actuated anchors and spring-loaded position transducers connected in series by extendable rods. These anchors were located at depths close to the ground surface, boundary between the soil and rock layers and the bottom end of the pile. And the transducers tracked the relative movements among the three anchors.

4.2 High-strain dynamic test

Two more bored piles of the same diameter but with slightly different depths of 56.70 and 52.40 m were also constructed. High-strain dynamic load (PDA) tests namely PDA01 and PDA02 were performed on these additional piles in November 2020. The

bored pile associated with PDA01 test was located just off BH-02 borehole, while that of PDA02 test was 6 m away as shown in Fig. 2. It is noteworthy that the average concrete compressive strengths at 28 days for both additional bored piles were 32 MPa. A strain gauge and an accelerometer were attached on the surface of each pile approximately 1 m below the head. A hammer 270 kN in weight was allowed to freely drop 2.10 m to impact the pile head, thus creating force waves in the pile. The installed strain gauge and accelerometer allowed for monitoring of the force wave-time and wave velocity-time relations in the pile. These experimental data were later analyzed by the notable CAPWAP software [10].

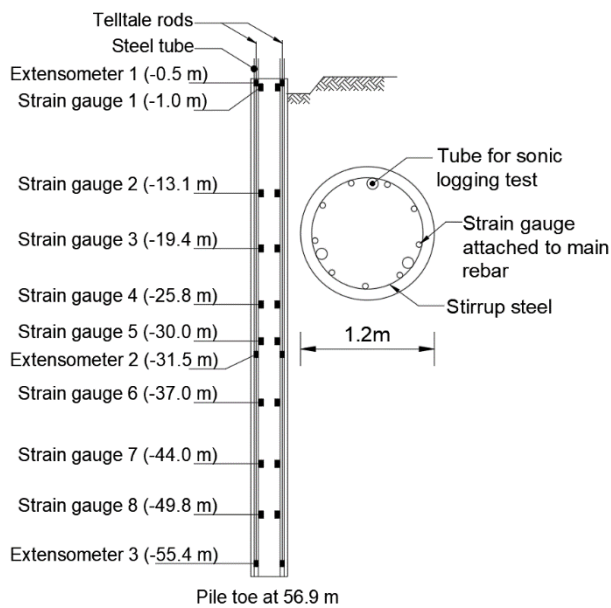


Fig. 4 Installation of vibrating-wire strain gauges and extensometers in test bored pile

5. Field test results

5.1 Load-settlement relations as determined from static load test

The load-settlement relations of the static load test are presented in Fig. 5. It can be observed that the pile response is inelastic exhibiting permanent settlements after unloading of each cycle. For the first cycle, the settlement of the pile at $P = P_a$ is 8.20 mm and a permanent settlement of 3.50 mm is present. The maximum settlement of Cycle 2, in which $P = 2P_a$, is 17.10 mm. The observed permanent settlement for this case is 5.20 mm.

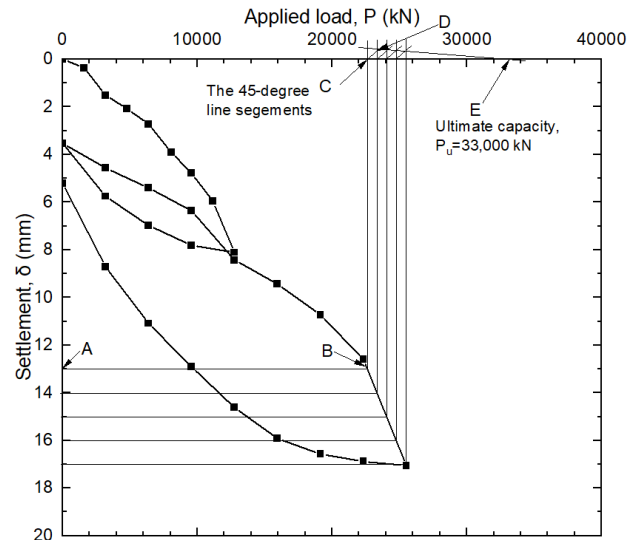


Fig.5 Load-settlement relations obtained from static load test

It should be noted that hysteresis is clearly present in the unload-reload portions of the $P - \delta$ curve. It is apparent that the pile ultimate capacity could not be reached during the pile load test. In an attempt to approximate this quantity, the graphical procedure recommended by [11] is followed. For the last load step of Cycle 2, horizontal lines (AB) with even intervals are drawn, intersecting the experimental $P - \delta$ curve as shown in Fig. 5. Vertical lines (BC) are further drawn from these points of intersection to the top horizontal or P -axis. A set of lines (CD) inclined by 45° are then placed intersecting the adjacent vertical lines. The ultimate capacity (Point E) can finally be determined as the intersection point of the straight line (DE) connecting all the points of intersection of the adjacent vertical lines to the P -axis. Based on this procedure, an ultimate capacity of 32,500 kN is approximated for the present static load test.

5.2 Load-settlement relations as determined from PDA tests

The force wave-time and wave velocity-time data were recorded using Pile Dynamic Analyzer Model PAX 8 and the onboard CAPWAP software further analyzed the load-settlement response. The CAPWAP analysis is based on numerical solution of the 1D governing force wave equation of an assumedly homogeneous elastic pile subject to an impact load at the head. Nonlinear pile-soil response represented by a soil damping factor and pile impedance is accounted for in the calculation of the pile capacity and settlement. The pile axial force is calculated based on the measured velocity. Such a calculated force is then compared to the measured force determined from strain gauge readings. The calculation is readjusted until the

difference between the calculated and measured forces is within a tolerance. The load-settlement relations obtained from the CAPWAP analysis are presented in Fig. 6. It can be observed that the PDA results are in good agreement with the primary loading portions of $P - \delta$ relations obtained from the static load test. The predicted ultimate pile capacities for PDA01 and PDA02 tests are 31,700 kN and 34,300 kN, with maximum settlements of 27.40 mm and 29.90 mm, respectively. It should be noted that the predicted ultimate capacity of PDA01 test of 31,700 kN is practically identical to the extrapolated capacity of the static load test of 32,500 kN. Further note that PDA01 test is more comparable to the static load test due to the piles' close depths.

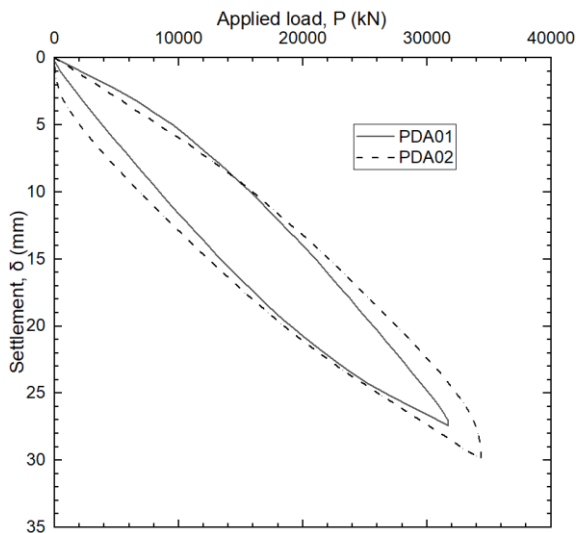


Fig. 6 Load-settlement relations determined from PDA tests

5.3 Load transfer along pile depth

The strain gauge readings can be converted to pile axial loads using the following mathematical expression:

$$P = \varepsilon EA \quad (1)$$

where P is the pile axial load; ε is the strain gauge reading; E is the pile elastic modulus and A is the cross-sectional area of the pile. In engineering practice, the elastic modulus of a bored pile is generally assumed to be equal to that of the concrete. However, bored piles are, in fact, composite material comprising of concrete and reinforcing steel. The elastic modulus determined based on the compressive strength of concrete alone is inaccurate due to the material nonlinearity under compressive loads [12].

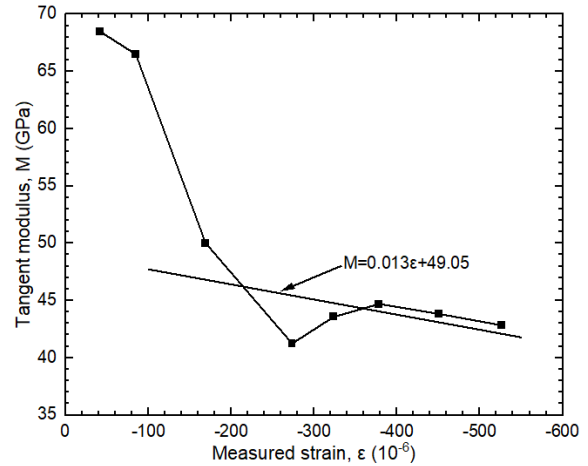


Fig. 7 Variation of pile tangent modulus and measured strain at the first strain gauge level

Fellenius (1989) [13] introduced a simple yet widely used method to determine the elastic modulus of reinforced concrete piles. The tangent elastic modulus (M) is first determined as the ratio between a change in stress from one load step to the next ($\sigma_{n+1} - \sigma_1$) and the corresponding change in strain reading ($\varepsilon_{n+1} - \varepsilon_1$). In this application, the stresses are determined from the known applied loads in the pile portion above excavation level or the top part of an embedded pile in which skin friction is very small and the corresponding axial load transfer is negligible. The calculated values of tangent modulus are then plotted against the measured strains. In general the modulus-strain curve converges to a straight line whose slope is denoted by a and whose intercept to the tangent modulus or M -axis is denoted as b . This linear relationship can be written as:

$$M = \frac{d\sigma}{d\varepsilon} = a\varepsilon + b \quad (2)$$

where P is the pile axial load; ε is the strain gauge reading; Integrating Eq. 2, one obtains the pile's stress-strain relations, i.e.,

$$\sigma = \frac{a}{2} \varepsilon^2 + b\varepsilon \quad (3)$$

The elastic secant modulus E can be determined from Hooke's law of elasticity that is $\sigma = E\varepsilon$ as $E = \sigma/\varepsilon$. It follows from Eq. 3 that

$$E = \frac{a}{2} \varepsilon + b \quad (4)$$

The variation of tangent elastic modulus with strain reading of the first strain gauge level (Fig. 4) is shown in Fig. 7. It can be

observed that the values of tangent modulus sharply decrease and later decrease only marginally with increasing strain. The values of a and b that result in best fit to the “linear tail” of the $M - \varepsilon$ curve are found to be 0.013 and 49.05. The values of secant elastic modulus E calculated from these a and b values (per Eq. 4) are then employed to determine the pile axial forces at various pile depths and load steps (per Eq. 1). The results so obtained are presented in Fig. 8.

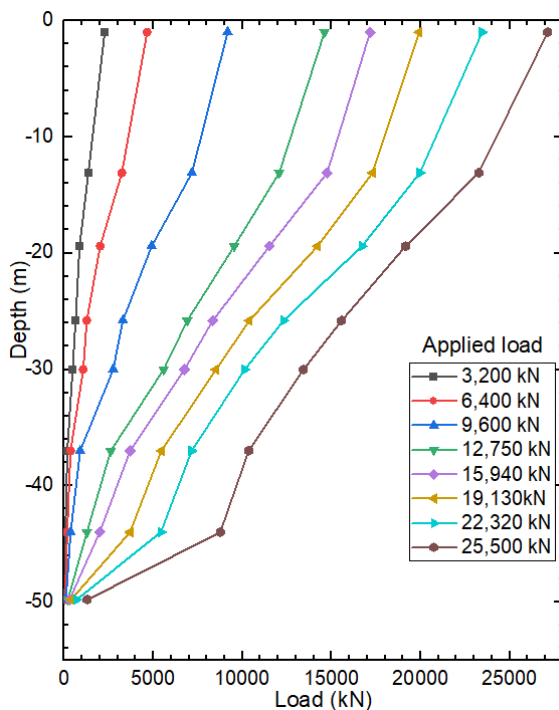


Fig. 8 Variation of pile axial loads for different load steps

The axial load-depth curves are noticeably nonlinear and rapidly decrease with depth. Towards the lower end, relatively small axial loads remain in the test pile. This clearly suggests that the friction along the pile’s shaft contributes to essentially all the mobilized pile capacity. At the design working load (P_d), the skin frictions of the soil layers account for as much as 60% of the capacity, while those of the rock layers are about 39%. These quantities become 55% for soil and 40% for rock, thus leaving end bearing of about 5% at $P=P_d$. The key implication of these findings is that both soil and rock skin frictions make up a significant portion of the total mobilized capacity and these should not be ignored when designing bored piles of comparable sizes in the subsoils of the Phnom Penh area. It is also apparent that full mobilization of the end bearing of such bored piles socketed in rock is practically impossible.

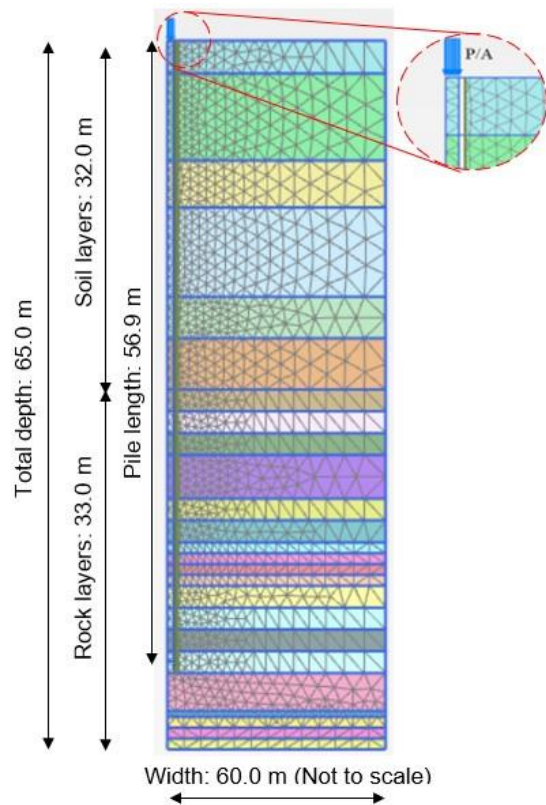


Fig. 9 Axisymmetric finite element model to simulate static load test

6. Finite element analysis of static pile load test

A two-dimensional finite element analysis was performed to simulate the pile behavior observed during the static load test. The finite element software Plaxis 2D Version 21 was adopted in such numerical simulation. As shown in Fig. 9, the axis-symmetric finite element model consists of a circular pile embedded in soil and rock layers so as to match the actual subsurface conditions of the test site. Isoparametric 15-noded triangular elements were employed in meshing of the model geometry. The elastoplastic Hardening Soil model and Hoek-Brown model were used to represent the soil and rock behavior. Interface elements were also employed to allow for slippage of the pile relative to the soils and rocks at their boundaries. The drainage conditions in the finite element analysis for the cohesive soil layers, cohesionless soil layers and rock layers were set to Undrained B, drained and non-porous, respectively. It is noteworthy that the pile was assumed to be linear elastic with a constant Young’s modulus value of 48.22 GPa, Poisson’s ratio of 0.25 and a unit weight of 25 kN/m³. Determination of the parameter values for the two constitutive models that result in fairly accurate simulation of the experimental $P-\delta$ relationships is presented in the subsections that follow.

6.1 Determination of parameter values for soil layers

The values of 14 parameters of the Hardening Soil model for the cohesive soils were mainly obtained from the laboratory test results. The values of E_{oed}^{ref} and OCR were calibrated from the one-dimensional consolidation tests, while E_{50}^{ref} and c' or s_u were determined from the stress-strain and strength relations of the unconfined compression tests and CU triaxial tests. The coefficient of lateral earth pressure at rest (K_0) was presumed to be unity and the total friction angle (ϕ) was set as zero for undrained analysis. The exponent m of 0.50 was found to result in best fit to the experimental results. The dilation angle (ψ) was assumed to be zero for all cohesive soil layers

It should be noted that, in the absence of laboratory strength test results, the correlation between undrained shear strength and N -value recommended by [9] particularly for the Phnom Penh cohesive soils was employed, that is

$$s_u = 5.5N \quad (5)$$

No results of triaxial tests with unload-reload cycles on intact specimens of Phnom Penh cohesive soils have been reported in the literature. Therefore, the values of unload-reload modulus used in the present finite element analysis were assumed based on comparable experimental studies on the mechanical behavior of Bangkok clay [14] and Ho Chi Min City clay [15]. It was found that $E_{ur}^{ref} = 4E_{50}^{ref}$ for soft cohesive soils and $E_{ur}^{ref} = 3E_{50}^{ref}$ for stiff cohesive soils resulted in best fit of the experimental load-settlement relations. The value of effective unload-reload Poisson's ratio (ν_{ur}) was assumed to be 0.20. for all cohesive soil layers.

For the case of cohesionless soils, the values of effective friction angle in the unit of degree were estimated using the empirical formula recommended by [16]:

$$\phi' = 27.1 + 0.3(N_1)_{60} - 0.00054[(N_1)_{60}]^2 \quad (6)$$

Where $(N_1)_{60} = C_N N_{60}$ is the effective stress-corrected N_{60} . According to [17] the correction factor C_N can be computed as:

$$C_N = \left[\frac{p_a}{\sigma'_v} \right]^{0.5} \quad (7)$$

In the above expression, $p_a = 100$ kPa is the atmospheric pressure and σ'_v is the vertical effective stress. The value of N_{60} is determined from N and equipment-specific correction factors:

$$N_{60} = \frac{\eta_H \eta_B \eta_S \eta_R N}{60} \quad (8)$$

In Eq. 8, η_H , η_B , η_S and η_R are the hammer efficiency, borehole-diameter correction, sampler correction and rod-length correction, respectively. The proper values of these standard efficiency and correction factors can be referred to [18]. The magnitudes of E_{50}^{ref} for sands have generally been suggested to be in a range of $2000 - 3000N$ [19]. In the present study, $E_{50}^{ref} = 2500N$ was assumed. The values of E_{oed}^{ref} were presumed to be equal to that of E_{50}^{ref} and E_{ur}^{ref} was taken as equal to $3E_{50}^{ref}$. In this numerical simulation, the dilatancy angle was determined as $\psi = \phi' - 30^\circ$ for $\phi' \geq 30^\circ$ and $\psi = 0^\circ$ when $\phi' < 30^\circ$. Similar to the case of cohesive soils, the values of Poisson's ratio for all cohesionless soil layers were assumed to be 0.20. The value of asymptotic strength ratio for the Hardening Soil model (R_f) was set as 0.90. The parameter values of the Hardening Soil model that resulted in best fit to the experimental load-settlement results are summarized in Table 1.

6.2 Determination of parameter values for rock layers

The Hoek-Brown model employs eight parameters in the prediction of stress-strain and strength behavior. The value of modulus of rock mass can be calculated as per the recommendation of [20]:

$$E_{rm} = jM_R \sigma_{ci} \quad (9)$$

where j is the rock mass factor; M_R is the ratio of the elastic modulus of the intact rock to its unconfined compression strength and σ_{ci} is the unconfined compression strength.

Table 1 Parameter values for Hardening Soil model for upper soil layers.

Material	Depth (m) From - To	γ_{sat} (kN/m ³)	γ_{unsat} (kN/m ³)	E_{50}^{ref} (kN/m ²)	E_{oed}^{ref} (kN/m ²)	E_{ur}^{ref} (kN/m ²)	OCR	K_0	ν_{ur}	p_{ref} (kN/m ²)	c' (kN/m ²)	ϕ' (deg.)	ψ (deg.)	m	R_f
Layer 1: Loose silty SAND (SM)	0.0 – 3.0	18.93	15.30	4,167	4,167	12,500	1.00	0.520	0.2	100	0.00	28.66	0	0.5	0.9
Layer 2: Firm to stiff lean CLAY (CL)	3.0 – 11.0	18.81	14.67	3,508	4,167	10,520	1.72	1.00	0.2	100	60.27	0	0	0.5	0.9
Layer 3: Soft to firm fat CLAY (CH)	11.0 – 15.3	16.48	11.09	3,755	1,648	11,270	1.00	1.00	0.2	100	22.10	0	0	0.5	0.9
Layer 4: Stiff to very stiff sandy lean CLAY (CL)	15.3 – 23.5	19.35	15.48	2,703	3,763	8,108	1.10	1.00	0.2	100	104.10	0	0	0.5	0.9
Layer 5: Medium dense to dense silty SAND, silty-clayey SAND (SM)-(SC-SM)	23.5 – 27.3	20.36	17.51	2,6250	2,6250	78,750	1.00	0.406	0.2	100	0.00	36.43	6.43	0.5	0.9
Layer 6: Very stiff to very hard lean CLAY (CL)	27.3 – 32.0	20.50	17.43	6,368	5,249	19,100	1.10	1.00	0.2	100	189.90	0	0	0.5	0.9

Note: γ_{sat} - soil unit weight below phreatic level, γ_{unsat} - soil unit weight above phreatic level, E_{50}^{ref} - secant stiffness in standard triaxial test, E_{oed}^{ref} - tangent stiffness for primary oedometer loading, E_{ur}^{ref} - unloading/reloading stiffness from triaxial test, OCR - overconsolidation ratio, K_0 - coefficient of lateral earth pressure at rest, ν_{ur} - Poisson's ratio, p_{ref} - reference stress for stiffness, c' - effective cohesion (effective analysis) or $s_{u,ref}$ - undrained shear strength (total analysis), ϕ' - effective friction angle, ψ - dilatancy angle at failure, m - modulus exponent for stress dependency, R_f - failure ratio

Table 2 Parameter values for Hoek-Brown model for rock layers.

Material	Depth (m) From - To	γ_{sat} (kN/m ³)	γ_{unsat} (kN/m ³)	E_{rm} (MPa)	ν	σ_{ci} (MPa)	m_i	GSI	D
Layer 7a: Completely weathered CLAYSTONE	32.0 - 34.0	23.50	23.50	10.86	0.30	2.30	4	8	0
	34.0 - 36.0	23.50	23.50	7.07	0.30	2.30	4	6	0
	36.0 - 38.0	23.50	23.50	8.76	0.30	2.30	4	7	0
	38.0 - 42.0	23.50	23.50	7.07	0.30	2.30	4	6	0
Layer 7b: Highly weathered SANDSTONE	42.0-44.0	24.50	24.50	8.49	0.25	4.60	17	16	0
	44.0 - 46.0	24.50	24.5	13.03	0.25	4.60	17.0	19	0
Layer 8a: Moderately weathered SANDSTONE-CLAYSTONE	46.0 - 47.0	24.50	24.50	246.6	0.25	15.70	17	44	0
	47.0 - 48.0	24.74	24.74	257.44	0.25	16.39	17	44	0
	48.0 - 49.0	25.24	25.24	753.67	0.25	25.24	17	53	0
	49.0 - 50.0	24.39	24.39	600.49	0.25	20.11	17	53	0
	50.0 - 52.0	24.39	24.39	29.32	0.25	7.35	17	33	0
	52.0 - 54.0	24.39	24.39	16.80	0.25	7.35	17	28	0
	54.0 - 56.0	25.24	25.24	195.24	0.25	26.87	17	37	0
	56.0 - 58.0	24.77	24.77	119.56	0.25	27.51	17	33	0
Layer 8b: Slightly weathered SANDSTONE	58.0 - 61.5	25.77	25.77	985.08	0.25	32.99	17	53	0
	61.5 - 62.0	26.43	26.43	2,104.02	0.25	56.88	17	65	0
	62.0 - 63.0	25.50	25.50	1,524.06	0.25	46.85	17	64	0
	63.0 - 64.0	24.56	24.56	1,120.35	0.25	34.44	17	64	0
	64.0 - 65.0	25.74	25.74	2,053.37	0.25	44.81	17	71	0

Note: γ_{sat} - rock unit weight below phreatic level, γ_{unsat} - rock unit weight above phreatic level, E_{rm} - deformation modulus of a jointed rock mass, ν - Poisson's ratio, σ_{ci} - uni-axial compression strength of the intact rock, m_i - intact rock parameter, GSI - Geological Strength Index

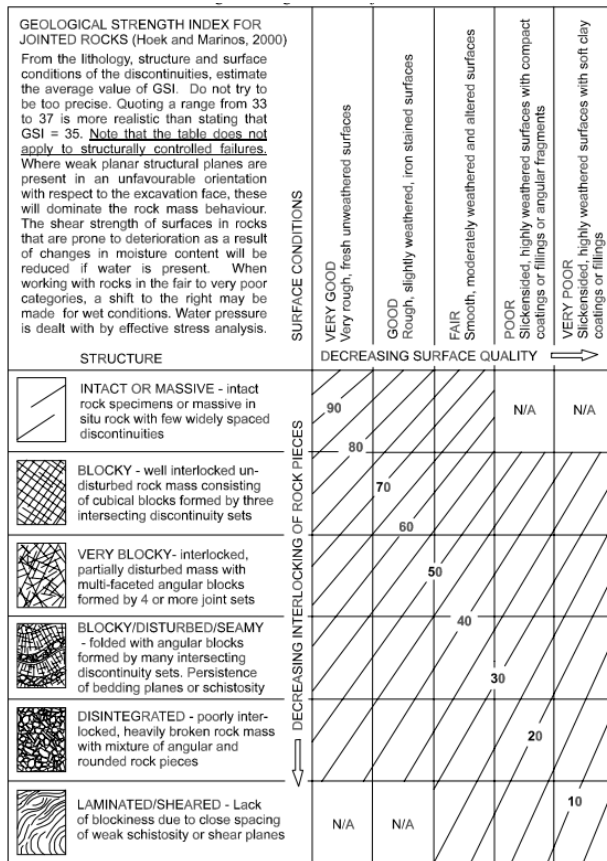


Fig. 10 Chart to determine geological strength index for rock mass [20]

Zhang and Einstein (2004) [21] suggested an empirical relationship for the mass factor:

$$j = 10^{0.186RQD-1.91} \quad (10)$$

The parameter RQD is the rock quality designation. M_R values in a range of 150-300 have been suggested for poorly cemented to highly cemented sandstone [20]. For claystone, M_R in a range of 200-300 have been recommended [22]. The sandstone samples obtained from the test site exhibited poor cementation, the M_R value was thus assumed to be 150, and the M_R value for claystone used in this finite element analysis was taken as 250. The value of intact rock parameter (m_i), in general, varies with the type of rock. Marinos and Hoek (2000) [23] recommended m_i values in ranges of 13-21 and 2-6 for sandstone and clay stone. In the present study, m_i values of 17 and 4 were assumed for sandstone and claystone, respectively.

The geological strength index (GSI) is one of the key factors that control the predicted stress-strain and strength behavior of rock according to Hoek-Brown model. The value of GSI depends on both integrity of the rock structure and its surface

condition. Suitable GSI values can be graphically obtained from the design chart [23] in Fig. 10. The disturbance factor (D) is a dimensionless input parameter that controls the shape of the failure surface. Its value depends on the state of disturbance that, in turn, varies with the stress relaxation and expansion of the rock mass undergoing excavation. $D = 0$ indicates no disturbance, while D of unity suggests severe disturbance. In this numerical study, D was taken as zero based on the observed slight deformations of the rock mass during the drilling process of the pile. The values of Poisson's ratio for all rock layers were assumed to be 0.25.

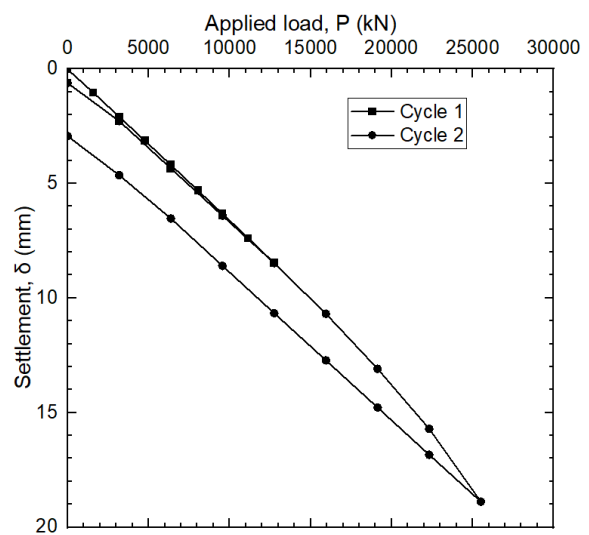


Fig. 11 Load-settlement relations as obtained from finite element analysis

The parameter values of the Hoek-Brown model that resulted in best fit to the experimental load-settlement results are summarized in Table 2. It is noteworthy that a stiffness-strength reduction factor (R_{inter}) value of 0.90 was assumed for all interface elements at the boundaries of the pile and the soil and rock layers.

7. Results of finite element analysis

The load-settlement relations obtained from the finite element analysis are presented in Fig. 11. Similar to the experimental results, the numerical $P-\delta$ curves are also nonlinear. However, the hysteretic unload-reload loop observed in the field load test cannot be simulated by the finite element model as an isotropic hyperelastic relation is used in the element-level calculation of stresses from the corresponding elastic strains. The trends of permanent settlements at the pile head increasing with maximum test

loads can be captured. This indicates slippage between the elements of the foundation materials relative to the pile along the provided interface elements as intended.

The numerical $P-\delta$ relations are plotted with the results of the static load test and PDA tests in Fig. 12. It can be observed that the finite element model together with the employed parameter values can simulate the load-settlement curve of the static load test with good accuracies, particularly for the primary loading of Cycle 1. For Cycle 2 beyond the maximum past load of Cycle 1, the finite element model produces slightly “softer” or conservative response, in that it predicts pile head settlements about 10% larger than the experimental values. It is also seen that the experimental permanent settlements after unloading are somewhat under-predicted by the finite element model for both load cycles.

It can be observed that the numerical axial forces inside the bored pile are somewhat greater than the experimental values for all depths considered. Therefore, the distributed skin frictions obtained from the finite element analysis are smaller than the actual capacities, and this renders larger numerical end bearings at the pile toe.

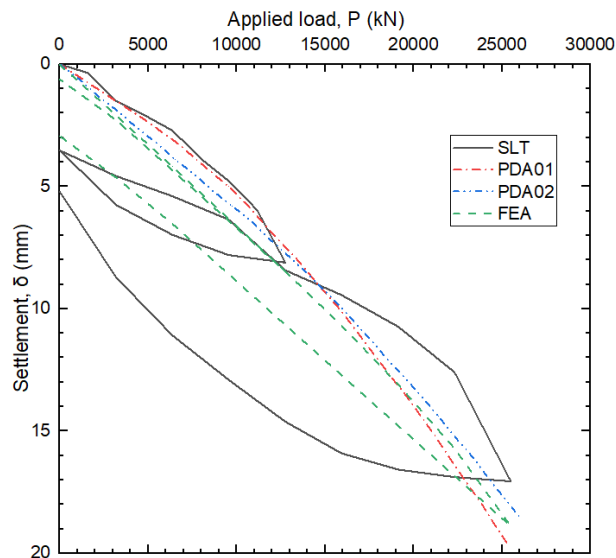


Fig. 12 Comparison of load-settlement relations obtained from static load test, PDA tests and finite element analysis

8. Conclusions

A static pile load test and high-strain dynamic (PDA) tests were performed on large-diameter bored piles socketed in sedimentary rock in the Phnom Penh area. The load-settlement relations and load transfer mechanisms observed from these

full-scale tests were analyzed. Axisymmetric finite element analysis of the static load test was also performed. Key findings of the present study can be summarized as follows:

1. The load-settlement relations obtained from the static load test and PDA tests were in excellent agreement. The extrapolated ultimate capacity of the static load test was also found to be practically identical to that predicted by the comparable PDA test. This suggests potential use of the PDA test, particularly in design practice, to cross-check the response of axially bored piles socketed in rock in the Phnom Penh area.
2. It was observed that both soil and rock skin frictions contributed to a significant portion of the total mobilized capacity. As such they should not be ignored in analysis and design of the load bearing capacity of bored piles comparable to the present test piles.
3. It appears that full mobilization of the end bearing of such large-diameter bored piles is very difficult or practically impossible to attain. The actual ultimate capacity is thus not known. This, not surprisingly, compromises the accuracy and level of confidence of the conventional limit-analysis design methods. A verifiable and more relevant means to design such piles socketed in rock should be based on performance or settlement criteria in which a safe working load is established so as to ensure an acceptable corresponding head settlement of the pile and the superstructure.
4. The axisymmetric finite element model together with the employed values of the constitutive models' parameters was able to simulate the load-settlement relations of the static load test rather accurately. This implies that finite element analysis, using increasingly accessible commercial software and with sound understanding of the pile-soil fundamental behavior of the designer, can potentially be performed to establish a safe working load of the bored pile based on performance or settlement criteria in these typical ground conditions.

Even though the parameter values of the Hardening Soil model and Hoek-Brown model for the typical soil and rock layers in the Phnom Penh area have primarily been proposed in the present study, the authors recommend more extensive laboratory and in-situ experimental programs be undertaken.

This will help develop a reliable and robust database on the mechanical behavior of the local foundation materials. Such information will be highly instrumental for successful calibration of proper constitutive models used in realistic performance-based finite element analyses of deep foundations in the Phnom Penh area.

Acknowledgement

The static load test and PDA test data presented herein were provided by Inros Lackner (Cambodia) Co., Ltd. The authors wish to thank Mr. Rainer Ernst Israel, Director of Inros Lackner (Cambodia) Co., Ltd., and the staff engineers of the company for encouraging this study on foundation design practice of the Phnom Penh area.

References

- [1] Pells P. J. N., Rowe R. K. and Turner R. M. (1980). An experimental investigation into side shear for socketed piles in sandstone. *International Conference on Structural Foundation on Rock*, Sydney Australia, pp.291-302.
- [2] Horvath R. G., Kenny T. C. and Kozicki, P. (1983) Methods for improving the performance of drilled piers in weak rock. *Canadian Geotechnical Journal*, 20(4), pp.758-772.
- [3] Liu, X., Bai, X., Zhang, M., Wang, Y., Sang, S., & Yan, N. (2020). Load-bearing characteristics of large-diameter rock-socketed piles based on ultimate load tests. *Advances in Materials Science and Engineering*, 2020, pp.1-12.
- [4] Xing, H., Wua, J., & Luo, Y. (2017). Field tests of large-diameter rock-socketed bored piles based on the self-balanced method and their resulting load bearing characteristics. *European Journal of Environmental and Civil Engineering*, 23(12), pp.1-15.
- [5] Ayithi, A., & Ryan, W. G. (2019). Unit side shear in rock-socketed bored piles. *Stress Wave Theory and Testing Methods for Deep Foundations: 10th International Conference, ASTM STP1611*, West Conshohocken, PA, pp.97-127
- [6] Chen, Xy., Zhang, My. and Bai, Xy (2019). Axial resistance of bored piles socketed into soft rock. *KSCE Journal of Civil Engineering*, 23, pp.46-55.
- [7] Aye, Z. Z., Boonyarak, T., Thasnanipan, N. and Chea, S. (2017). Performance of large-diameter bored pile socketed in sandstone and siltstone in Thailand. *The DFI-PFSF 2017 Conference*, Melbourne, 21-22 March 2017, pp.35-44.
- [8] Haberfield C. M. and Lochaden A. L. E. (2019). Analysis and design of axially loaded piles in rock. *Journal of Rock Mechanics and Geotechnical Engineering*, 11, pp.535-548
- [9] Touch, S., Likitlersuang, S. and Pipatpongsa, T. (2014). 3D geological modelling and geotechnical characteristics of Phnom Penh subsoils in Cambodia. *Engineering Geology*, 178, pp.58-69.
- [10] Rausche F., Goble G. G. and Likins, G. E. (1984). Dynamic determination of pile capacity. *Journal of Geotechnical Engineering*, 111(3), pp.367-383.
- [11] Mazurkiewicz, B. K. (1972). *Test loading of piles according to polish regulations. Preliminary Report No. 35*, Commission on Pile Research, Royal Swedish Academy of Engineering Service, Stockholm.
- [12] Krasinowski, A. and Wiszniewski, M. (2017). Static load test on instrumented pile – field data and numerical simulations. *Studia Geotechnica et Mechanica*, 39(3), pp.17-25. doi:10.1515/sgem-2017-0026
- [13] Fellenius, B. H. (1989). Tangent modulus of piles determined from strain data. *The American Society of Civil Engineers, ASCE, Geotechnical Engineering, Division, 1989 Foundation Congress*, F. H. Kulhawy, Editor, pp.500-510.
- [14] Surarak, C., Likitlersuang, S., Wanatowski, D., Balasubramaniam, A., Oh, E. and Guan, H. (2012). Stiffness and strength parameters for hardening soil model of soft and stiff Bangkok clays. *Soils and Foundations*, 52(4), pp.682-697.
- [15] Trung, N. D. (2019). Determination of the unloading - reloading modulus and exponent parameters (m) for hardening soil model from drained triaxial test of soft soil in Ho Chi Minh City. *Modern Environmental Science and Engineering*, 5(1), pp.207-216. doi:10.15341/mese(2333-2581)/01.05.2019/001
- [16] Peck, R. B., Hanson, W. E., & Thornburn, T. H. (1974). *Foundation engineering* (2 ed.). New York: John Wiley & Sons.
- [17] Liao, S. S. C. and Whitman, R. V. (1986). Overburden correction factors for SPT in sand. *Journal of Geotechnical Engineering*, 112(3), pp.373-377.
- [18] Salgado R. (2008). *The Engineering of Foundations*. The McGraw Hill Companies.
- [19] Ou, C.-Y. (2021). *Fundamentals of Deep Excavations*. The Netherlands: CRC Press.

- [20] Tomlinson, M., & Woodward, H. (2015). *Pile Design and Construction Practice* (6 ed.) .CRC Press.
- [21] Zhang, L. and Einstein, H. H. (2004). Using RQD to estimate the deformation modulus of rock masses. *International Journal of Rock Mechanics & Mining Sciences*, 41, pp.337–341. doi:10.1016/S1365-1609(03)00100-X
- [22] Hoek, E. and Diederichs, M. S. (2006). Empirical estimation of rock mass modulus. *International Journal of Rock Mechanics and Mining Sciences*, 43(2), pp.203-215. doi:https://doi.org/10.1016/j.ijrmms.2005.06.005
- [23] Marinos, P. and Hoek, E. (2000). GSI — A geologically friendly tool for rock mass strength estimation. *The ISRM International Symposium*, Melbourne, Australia.